




Fast-kinetics adsorption of a binary solution containing cationic and ionic pollutants using high-surface area activated carbon derived from macadamia nutshell

Estefania Duque-Brito¹ · Diego Ramón Lobato-Peralta¹ · Jude A. Okolie² · Dulce Maria Arias¹ · Pathiyamattom Joseph Sebastian¹ · Patrick U. Okoye¹ 

¹ Instituto de Energías Renovables (IER-UNAM), Privada Xochicalco s/n, 62580 Temixco, Morelos, México

² Gallogly College of Engineering, University of Oklahoma, Norman, OK 73019, USA

Received: 11 July 2023 / Revised: 24 October 2023 / Accepted: 25 October 2023 / Published online: 18 November 2023

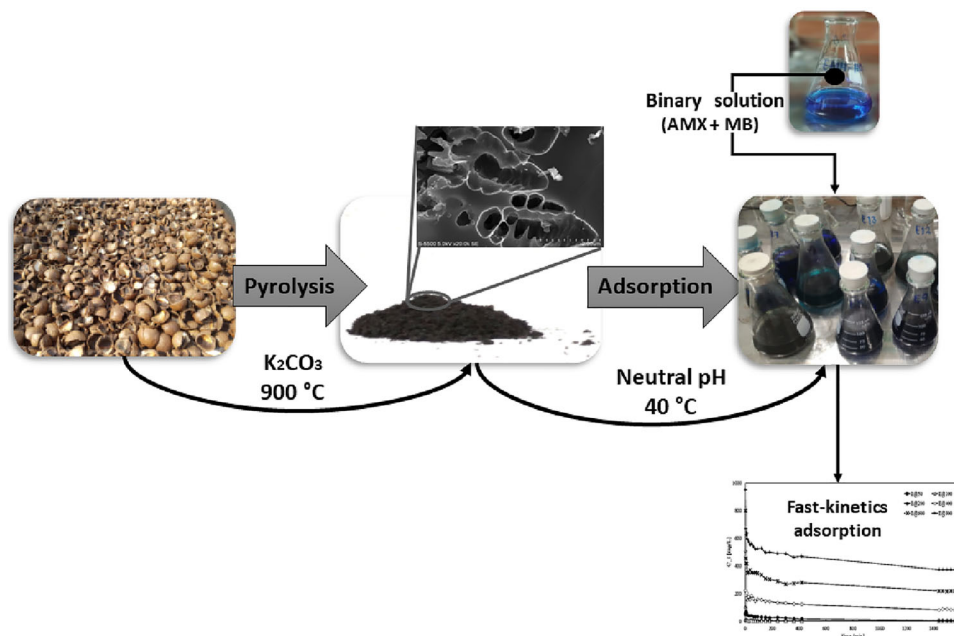
© The Author(s) 2023

Abstract Wastewater is characterized by multipollutant, and the presence of competitive adsorption could affect removal efficiency. Hence, the decontamination of water by adsorption in a multicomponent system allows an understanding of the practically and adsorbent efficiency. In this study, we present an analysis of the adsorption phenomena in a binary solution comprising compounds from distinct families, a dye, and an antibiotic, utilizing activated carbon obtained through a sustainable procedure. Locally available agricultural biowaste, specifically macadamia nutshell (MNS), served as a sustainable precursor to produce hierarchical porous activated carbon. The activation conditions were fine-tuned using the Box–Behnken experimental design. The resultant activated carbon was employed to remove a binary solution (BS) comprising the cationic dye, methylene blue (MB) and an ionic molecule amoxicillin (AMX) under specified conditions, including a pH range of 2 to 12, an initial concentration of BS ranging from 50 to 800 mg/L, and an adsorbent dosage within the range of 0.1 g to 0.3 g in a single adsorption system. The

results revealed that higher temperatures adversely impacted the carbon yield, with a pronounced interaction effect observed between temperature and time. The activation temperature and K_2CO_3 :precursor molar ratio predominantly influenced the textural and morphological properties of the activated carbon. Under optimal conditions (900 °C, 1 h, and a K_2CO_3 :precursor ratio of 2:1), remarkably high-surface area (1225 m²/g), pore volume (0.801 cm³/g), and a nanopore size of 0.406 nm were achieved. In binary adsorption studies, R2-MNS demonstrated a maximum adsorption capacity of 578.925 mg/g. A pH above 4.5 produced an antagonistic effect on the removal of AMX due to competitive adsorption. Evaluation of three isotherm models demonstrated that the Khan isotherm best describes the affinity of BS to R2-MNS. The pseudo-second-order kinetic model best describes the data, indicating a chemisorption mechanism. The interparticle diffusion test revealed that the adsorbent exhibited very fast adsorption behaviour at the initial stage.

✉ Patrick U. Okoye
ugopaok@ier.unam.mx

Graphical abstract



Keywords Methylene blue · Amoxicillin · Optimization · Potassium carbonate · Green chemistry

1 Introduction

Presently, research on activated carbon development is closely associated with the investigation of various precursors, including agricultural wastes (Leite et al. 2018; Nworie et al. 2022; Malesic-Eleftheriadou et al. 2022; Liu et al. 2023), invasive forest fruits or trees (Lazarotto et al. 2022), and their interaction with contaminants present in the environment. Nevertheless, the core issue lies in the composition of water, as contaminated water harbours a mixture of pollutants resulting from industrial discharges, untreated agricultural runoff, and domestic waste (da Silva Santos et al. 2021; Ismail et al. 2022). Therefore, it is crucial to direct activated carbon research towards addressing the simultaneous removal of numerous pollutants, rather than considering it as an ideal scenario with controlled variables. In this regard, only a limited number of studies have undertaken the formidable challenge of addressing this issue. For instance, Aichour and Zaghouane-Boudiaf (2020) discussed the mechanism of adsorption using two cationic dyes as pollutants from single and binary solutions onto activated carbon from citrus peel. Yazidi et al. (2020) studied the competitive adsorption phenomenon using durian shell as a precursor for activated carbon to adsorb amoxicillin and tetracycline.

They obtained a better adsorption capacity for amoxicillin than tetracycline using their material. Chandrasekaran et al. (2020) prepared activated carbon from *Prosopis juliflora* wood for ciprofloxacin and amoxicillin adsorption in single and binary systems. They revealed that ciprofloxacin has an antagonistic effect on amoxicillin adsorption in binary system. Other studies have reported the use of lignocellulosic biomass such as, avocado seed (Zhu et al. 2018), coconut shell (Qin et al. 2018), a mixture of almond and apricot stone shell (Kılıç and Orhan 2019), tree pods from *Erythrina speciosa* (Bouzidi et al. 2023) to carry out binary adsorption of pollutants simultaneously or in parallel. Furthermore, removing contaminants from water has been elucidated theoretically using density functional theory to simulate the interaction of water molecule and contaminants considering Van der Waals dispersion interaction (Nematov et al. 2022).

Contaminants include heavy metals, rare earth metals (Iftekhar et al. 2022), or organic molecules that exist as cationic, anionic, or ionic species upon contact with water. The challenge lies in the fact that the efficiency of the adsorbent for a specific pollutant (be it cationic, anionic, or an ionic molecule) depends on factors such as the precursor used, textural characteristics, and the presence of functional groups (carboxylic, phenolic, quinones) on the surface of the activated carbon (Nayagam and Prasanna 2022). This implies that multiple activated carbons would be necessary for each type of pollutant, leading to a cost-intensive process of pollutant removal using activated carbons. However, parallel adsorption using a single adsorbent has shown that, in addition to the mentioned

functional groups, the presence of heteroatoms like nitrogen, sulphur, phosphorus, and even trace inorganic elements in the carbon could enhance the removal of more than one pollutant (Figueiredo and Pereira 2012; Sun et al. 2019). Moreover, the implementation of binary adsorption involving both anions and cations can contribute to a better understanding of the mechanisms governing the selection process when activated carbon interacts with pollutants of varying polarities.

The development of multifunctional activated carbon from abundant lignocellulosic biomasses, capable of simultaneous multi-pollutant adsorption, has the potential to enhance overall wastewater secondary and tertiary treatment processes. Macadamia nutshell, a lignocellulosic biomass considered as residue, constitutes approximately one-third of the total mass of the fruit. In Mexico, the production of macadamia nuts in 2021 reached 21.58 tons per hectare, contributing to a total production of approximately 32,205.77 tons of this product (Servicio de Información Agroalimentaria y Pesquera 2023). Likewise, the worldwide production was about 369,491 tons in the same year (SAMAC. Macadamias South Africa NPC 2023). Therefore, the substantial production of macadamia nuts has resulted in a significant quantity of residual shells. Limited studies have reported the utilization of activated carbon derived from macadamia nutshell, primarily focusing on the removal of a single pollutant. This adsorbent has predominantly been employed for the removal of dyes and tetracycline. For instance, Martins et al. (2015) prepared activated carbon from macadamia nut shells using NaOH as an activating agent for the removal of tetracycline antibiotics, obtaining a maximum adsorption capacity of 455.33 mg/g. Dao and Le Luu (2020) activated macadamia nutshell using H_2SO_4 and K_2CO_3 for the removal of methylene blue in the water. Wongcharee et al. (2019) produced activated carbon from macadamia nutshell and zeolite composite via the physical activation method with CO_2 . The activated carbon was deployed to remove methylene blue (MB) from water. They reported a low maximum adsorption capacity of 97 mg/g. The same research group examined a common precursor, employing it as a hybrid magnetic nanosorbent material for the adsorption of synthetic melanoidin. Their findings revealed that the adsorbent achieved a capacity of 14.87 mg/g (Wongcharee and Aravinthan 2020). In contrast, Du et al. produced activated carbon from macadamia nutshell through KOH activation, utilizing microwave radiation for the adsorption of Reactive Blue 19 dye. Their results indicated that the material reached a maximum adsorption capacity of 376.81 mg/g (Du et al. 2017). Hence, the significance and novelty of our work lie in the fact that to the best of our knowledge, there is no available study on the removal of amoxicillin (AMX) using activated carbon

derived from macadamia nutshell. Besides, to the best of our knowledge there are no studies on the binary removal of methylene blue and amoxicillin using activated carbon from macadamia nutshell.

Antibiotics are used extensively to treat bacterial infections. According to World Health Organization (WHO), amoxicillin and amoxicillin/clavulanic acid are the most frequently consumed antibiotics globally (World Health Organization 2018). Similarly, AMX is used for veterinary bacterial infection treatment (Putra et al. 2009). The high demand for antibiotics has resulted in unregulated disposal, which could lead to drug resistance, skin irritation, nausea, stomachache, and diarrhea (Suárez and Gudiol 2009; Moura et al. 2018). Studies have shown that after the consumption of amoxicillin in humans, about $86 \pm 8\%$ is excreted through the urine (Pezoti et al. 2016). Moreso, high accumulation could result in an overdose, which is harmful to human beings and animals.

On the other hand, methylene blue (MB), with a chemical formula $C_{16}H_{18}ClN_3S$ is a cationic dye extensively used in the textile industry, surgical procedures, to treat some illnesses, and for veterinary purposes (Borghesi et al. 2021; Gupta et al. 2022). At high concentrations, MB could result in heart disease, skin irritation, vomiting, and headache and could be hazardous to the aquatic system (Al-Ghouti and Sweleh 2019; Xue et al. 2022). Hence, it is important to develop an effective adsorbent that is capable of removing both AMX and MB from aqueous solution in a binary system (Rodrigues et al. 2020).

To address the challenges associated with concurrently describing the adsorption of two pollutants in a binary solution using a sustainable adsorbent, we present the synthesis of activated carbon from macadamia nutshell. This process involves one-step chemical activation with K_2CO_3 as an environmentally friendly activating agent. The generated activated carbon was applied for the simultaneous removal of AMX and MB in a binary solution (BS). A comprehensive characterization of the developed activated carbon was conducted to elucidate the structural-performance relationship. The study involved the evaluation of the effects of pH, temperature, pollutant concentration, and contact time. Furthermore, the kinetics mechanism, three isotherm models, and the thermodynamics of the adsorption process were investigated.

2 Materials and methods

2.1 Materials

Amoxicillin, AMX ($C_{16}H_{19}N_3O_5S$, molecular weight = 365.40 g/mol) and methylene blue, MB ($C_{16}H_{18}ClN_3S$, molecular weight = 319.85 g/mol), were purchased from

Table 1 Levels of experimental factors in Box–Behnken design

Levels	K ₂ CO ₃ :Precursor (× 1)	Temperature, °C (× 2)	Activation time, h (× 3)
High (+ 1)	3:1	900	2
Medium (0)	2:1	800	1.5
Low (− 1)	1:1	700	1

Merck. HCl (98% purity), NaOH (99% purity), and K₂CO₃ anhydrous were all purchased from Sigma-Aldrich. The macadamia nutshell was provided to us by local farmers in Tepoztlán, Morelos, Mexico.

2.2 Activated carbon production

The experimental design employed the Box–Behnken approach to elucidate the impact of factors such as precursor:K₂CO₃ (× 1), activation temperature (× 2), activation time (× 3), and molar ratios on both the adsorption capacity of the binary solution (BS) and the carbon yield. The detailed experimental design is presented in Table 1. Box–Behnken designs are known for their efficiency and cost-effectiveness when compared to many 3^k factorial designs. The design allows for the selection of points from three-level factorial arrangements, and the experimental points can be situated on a hypersphere equidistant from the central points. Additionally, the use of an experimental design minimizes material waste and enables the use of milder conditions. Fifteen experimental runs were generated, with three of them being central points to measure the reproducibility and consistency of the data. The interaction factors and ANOVA analysis, with a model confidence level of 0.05 p-value, were elucidated.

Chemical activation was employed in the preparation of activated carbon from macadamia nutshell (MNS). Approximately 20 g of finely ground macadamia nutshell was impregnated with varying amounts of K₂CO₃ in a weight ratio ranging from 1:1 to 1:3 (K₂CO₃:precursor) in 200 mL of deionized water. The resulting slurry was heated to 85 °C for 4 h under vigorous stirring. Subsequently, the impregnated MNS with K₂CO₃ was dried at 105 °C in an oven overnight to eliminate excess moisture. Activation was carried out in an electrical tubular furnace (Linderberg Blue M) under a N₂ atmosphere (100 mL/min). Various conditions of temperature (ranging from 700 to 900 °C), with a heating rate of 20 °C/min, and residence time (between 1–2 h) were applied. The resultant carbon was washed with 1 M HCl to neutralize excess alkali salt and open the pores of the carbon. Following this, it was washed with deionized water until a neutral pH was achieved and subsequently dried in an oven at 105 °C for 2 h. The yield of the activated carbon was calculated using Eq. 1.

$$\text{Yield (\%)} = \frac{\text{MNS} - \text{AC}(g)}{\text{MNS}(g)} \times 100 \quad (1)$$

where MNS-AC (g), represents the resulting activated carbon of each run, and MNS (g) is the initial weight of the raw biomass.

2.3 Activated carbon characterization

The sample that presented the best behaviour was characterized by scanning electron microscopy (SEM) S-5500 (Hitachi) model series. The morphology was obtained at different magnifications from 15,000× to 50,000×. The elemental analysis was obtained using the energy dispersive X-ray spectroscopy (EDX, Bruker) attached to the SEM. Fourier transform infrared spectroscopy (FTIR, Nicolet iS50) was used to evaluate the functional groups associated with the adsorbent. The data was recorded in the wavenumber range from 4000 to 400 cm⁻¹. The nitrogen physisorption isotherm at 77 K was investigated using NOVA 2200e Quantachrome equipment. The specific surface area was calculated using Brunauer–Emmett–Teller (BET) and density functional theory (QS-DFT) models. The pore distribution was obtained using the QS-DFT method.

2.4 Batch adsorption experiments

The binary solution (BS) utilized to evaluate the adsorption capacity of the activated carbons comprised of an equal concentration of AMX and MB dissolved in deionized water. The experimental design was adapted from Wei et al. (2022). The conditions were tailored according to the adsorption capacity of the best-activated carbon sample, considering that the binary solution contains two pollutants. The total concentration was 400 mg/L, i.e. 200 mg/L of MB and 200 mg/L of AMX. The solution was refrigerated to avoid the degradation of AMX. Then, batch experiments were conducted by adding 100 mL of the 400 mg/L BS and 0.1 g of the MNSAC in Erlenmeyer flasks. The flasks were inserted in a thermostat shaker (Julabo-SW series) and were subjected to agitation at 150 rpm for 12 h at room temperature. Thereafter, the residual concentration was measured in a UV-visible spectrophotometer (Shimadzu UV-1900) at a range placed from 230 to 664 nm based on the calibration curve.

The percentage removal was calculated using Eq. 2.

$$\text{Removal } [\%] = \frac{C_0 - C_f}{C_0} \times 100 \quad (2)$$

where C_0 and C_f are the initial and final concentrations of BS in mg/L, respectively.

2.5 Influence of pH and pH_{pzc} value

The pH was evaluated by placing 200 mg/L of each pollutant, i.e. a total of 400 mg/L of BS and 0.1 g of the best activated carbon sample in Erlenmeyer flasks. The solution pH was adjusted using 0.1 M NaOH and 0.1 M HCl and left to equilibrate at 30 °C for 24 h under an agitation speed of 150 rpm. The initial and final pH was determined by a Sper Scientific Benchtop Meter potentiometer. The point of zero charge pH_{pzc} was determined where the initial pH (pH_i) intersects the final pH (pH_f), i.e. $\text{pH}_i = \text{pH}_f$.

2.6 BS adsorption equilibrium and kinetics studies

Equilibrium adsorption at different initial concentrations of the BS (50 mg/L to 800 mg/L) was conducted to investigate the adsorption kinetics. This was achieved by placing 200 mg/L of different BS concentrations in a flask and then adding 0.2 g of the best MNS-AC sample (this was determined from the adsorption capacity and the activated carbon yield). The solutions were heated at 30 °C for 24 h under constant agitation of 150 rpm. The removal with respect to time was determined by taking measurements at different time intervals. This procedure was repeated for different temperatures of 40 °C and 50 °C.

The amount of BS adsorbed at a time (t) in mg/g (q_t) was determined from Eq. 3.

$$q_t = \frac{(C_0 - C_t)V}{W} \quad (3)$$

where V (L) is the volume of the BS solution, W (g) is the weight of the activated carbon sample added, and C_t is the concentration at time t in mg/L. Also, using the concentration at the equilibrium (C_e) it is possible to calculate the quantity of BS adsorbed at the equilibrium in mg/g (q_e) as shown in Eq. 4.

$$q_e = \frac{(C_0 - C_e)V}{W} \quad (4)$$

Kinetics studies were estimated from q_e data and time t collected for each concentration of BS and were fitted to pseudo-first-order (PFO), pseudo-second-order (PSO), and Elovich models shown in Eqs. 5 (Lagergren 1907), 6 (Ho and McKay 1999), and 7 (Elovich and Larinov 1962).

$$\text{PFO}q_t = q_e(1 - e^{-k_1t}) \quad (5)$$

$$\text{PSO}q_t = \frac{k_2q_e^2t}{(1 + k_2q_e t)} \quad (6)$$

$$\text{Elovich}q_t = \frac{1}{\beta} \ln(\alpha\beta) + \frac{1}{\beta} \ln t \quad (7)$$

where, k_1 (1/min) and k_2 (g/mg·min) are the rate constants for PFO and PSO, respectively, at time t . The α and β are constants of the Elovich kinetics model, the first one refers to the initial adsorption rate, whereas the latter is the desorption constant. The interparticle diffusion by Weber and Morris (1962) was determined from Eq. 8.

$$q_t = k_p t^{1/2} \quad (8)$$

where t is the time in min and k is the constant intrinsic to the interparticle diffusion equation. To correlate the experimental data with PFO and PSO, all the values obtained were validated using the coefficient of determination R^2 (Eq. 9), root mean square error RMSE (Eq. 10), and average relative error ARE (Eq. 11).

$$R^2 = 1 - \frac{\sum_{i=1}^n (y_i - \hat{y}_i)^2}{\sum_{i=1}^n (y_i - \bar{y})^2} \quad (9)$$

$$\text{RMSE} = \sqrt{\frac{1}{n-1} \sum_{i=1}^n (y_i - \hat{y}_i)^2} \quad (10)$$

$$\text{ARE} = \frac{1}{n} \sum_{i=1}^n \left| \frac{y_i - \hat{y}_i}{y_i} \right| \quad (11)$$

2.7 Adsorption equilibrium isotherms

Experimental data from the kinetics studies were also used to analyse the adsorption isotherm models. To achieve this purpose, Origin software was used to find all the constants needed to fit experimental data to isotherms models. The models evaluated in this paper were Langmuir (1916) (Eq. 12), Freundlich (1906) (Eq. 13), and Khan (Eq. 14).

$$q_e = \frac{q_m k_L C_e}{1 + k_L C_e} \quad (12)$$

$$q_e = K_F C_e^{1/n_F} \quad (13)$$

$$q_e = \frac{q_m k_K C_e}{(1 + k_K C_e)^{n_K}} \quad (14)$$

where q_m is the maximum adsorption capacity of the adsorbent (mg/g), all K and n parameters refer to the equilibrium constant (L/mg) and dimensionless exponent from each isotherm, respectively. R is the universal gas constant (kJ/mol·K) and T corresponds to the temperature (K).

2.8 Adsorption thermodynamic parameters

Thermodynamic behaviour of the adsorption process and the interaction between BS and the best MNS-AC sample were investigated. The Gibbs free energy (ΔG°), enthalpy (ΔH°), and entropy (ΔS°) are calculated using the following Eqs. (15) and (16).

$$\Delta G^\circ = -RT \ln K_L \quad (15)$$

$$\ln K_L = \frac{\Delta S^\circ}{R} - \frac{\Delta H^\circ}{RT} \quad (16)$$

where K_L is the equilibrium constant from Langmuir isotherm, R is the ideal gas constant (8.314 J/mol·K), and T (K) is the temperature of the adsorption process.

3 Results and discussion

3.1 Effect of factors on the activation process over yield and BS adsorption

Response surface methodology, implemented with the Box–Behnken design, was employed to investigate the impact of activation factors on the yield and adsorption capacity of the BS. The obtained results revealed that the activation time and the K_2CO_3 :precursor molar ratio are not significantly influential in the model prediction, as indicated by the p -values obtained from ANOVA. Consequently, these factors do not significantly affect the adsorption of the BS and the yield of activated carbon,

Table 2 Extended Box–Behnken design matrix for K_2CO_3 chemical activation and the influence of factors over BS removal and yield

Run	× 1	× 2	× 3	Yield (%)	BS removal (%)
1	2:1	700	1	27.39	25.89
2	2:1	900	1	18.26	73.72
3	2:1	700	2	28.08	28.45
4	2:1	900	2	23.56	60.39
5	1:1	700	1.5	27.80	44.09
6	3:1	900	1.5	22.97	67.42
7	3:1	700	1.5	27.30	52.56
8	1:1	900	1.5	16.47	72.60
9	1:1	800	1	24.90	48.91
10	3:1	800	2	22.64	72.12
11	3:1	800	1	26.26	57.62
12	1:1	800	2	24.94	61.99
13	2:1	800	1.5	25.16	66.35
14	2:1	800	1.5	26.48	62.30
15	2:1	800	1.5	24.34	65.88

contrary to initial expectations. However, the activation temperature exhibited high significance in the model prediction, with a p -value of 0.004, which is lower than the 0.005 significance level. This signifies that the activation temperature significantly contributes to both the yield of activated carbon and the adsorption of the BS.

Factors interaction was very evident only for the BS adsorption, with the strongest interaction found for temperature–time. The Eqs. (17) and (18) represent the regression equation of the yield and BS adsorption, respectively.

$$\begin{aligned} \text{Yield} = & 25.33 + 0.633x_1 - 3.663x_2 + 0.302x_3 - 0.67x_1^2 \\ & - 1.03x_2^2 + 0.02x_3^2 + 1.75x_1x_2 - 0.91x_1x_3 \\ & + 1.15x_2x_3 \end{aligned} \quad (17)$$

$$\begin{aligned} \text{BSads} = & 64.84 + 2.77x_1 + 15.39x_2 + 2.1x_3 + 3.68x_1^2 \\ & - 9.36x_2^2 - 8.37x_3^2 - 3.41x_1x_2 + 0.36x_1x_3 \\ & - 3.97x_2x_3 \end{aligned} \quad (18)$$

The range of activated carbon yield found was from 16.47% (Run 8) to 28.08% (Run 3). For BS adsorption, the results varied from 25.89% (Run 1) to 73.72% (Run 2) (Table 2). Based on the removal percentage and low activating agent and activation time, Run 2 (R2-MNS) was selected. Besides, time and K_2CO_3 :precursor do not significantly influence the response variables and the model; therefore, it is not necessary to employ more resources, which will increase materials and operational costs. The central points (Run 13, 14, and 15) of the Box–Behnken 3^3 experimental design have a standard deviation of 1.081 for yield and 2.215 for BS adsorption. These values show good correlation, indicating consistency and reproducibility of the performance of the experiment.

3.2 Characterization of R2-MNS

The chemical composition of R2-MNS was determined by EDX analysis. The sample predominantly comprises of carbon (85.55%), followed by oxygen (7.78%), nitrogen (3.20%), silica (2.18%), and potassium (1.29%). It is noteworthy to mention that the impurities of silicon (Si) and potassium (K) likely originated from the intrinsic composition of the macadamia nutshell biomass and possibly from the activating agent. The micrographs of the R2-MNS at different magnifications were obtained from the SEM images. The 1500× micrograph (Fig. 1a) shows the porosity distribution throughout the R2-MNS surface. From Figs. 1b and c, it is possible to notice the non-homogeneous distribution of porosity of the sample of activated carbon. Additionally, the surface of R2-MNS

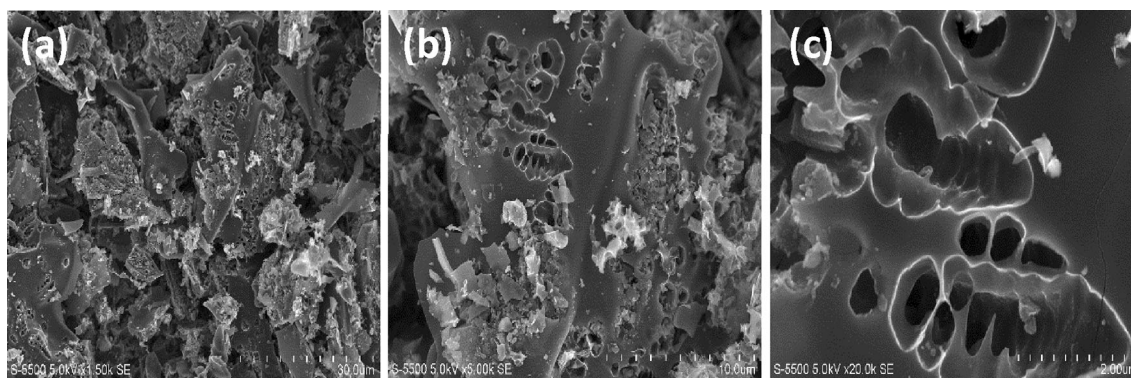


Fig. 1 Micrographs from SEM at: **a** 1500 \times , **b** 5000 \times and **c** 20,000 \times magnifications

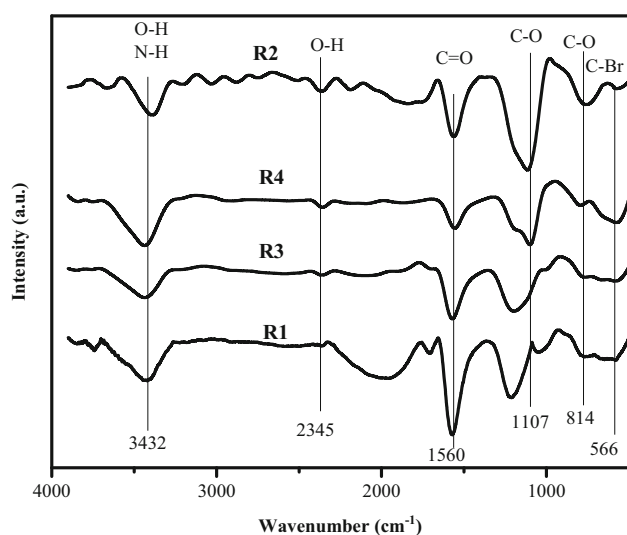


Fig. 2 FTIR spectra for macadamia nutshell activated carbon samples

exhibits slit pores and cracks, showcasing various types of pores. The white deposits observed on the surface correspond to inorganic elements, specifically silica and potassium, as indicated in the EDS analysis.

FTIR analysis presented in Fig. 2 showcases the spectra from R2 and R4, both exhibiting superior behaviour in terms of adsorption uptake and yield. Additionally, samples with lower adsorption and yield (R1 and R3) were included for comparative purposes. All four samples display a similar signal at $\sim 3430\text{ cm}^{-1}$, corresponding to the combined hydroxyl functional group and pyrrole (N–H) vibrations, as documented by Wong et al. (2018). Furthermore, the samples exhibit an intense response at $\sim 1560\text{ cm}^{-1}$, identified as the carboxyl functional group (C=O) (Lang et al. 2021). The peaks at 814 cm^{-1} and 1107 cm^{-1} are due to C–O bonding, typical carboxylic acids (Wei et al. 2022). However, for R1 and R3 at 1107 cm^{-1} , the peaks vibrate slightly out-of-phase compared to the best samples (R2 and R4). The mentioned

delay is caused by the displacement of the central atom of the functional group. In this case, the mentioned out-of-phase vibration could affect the interaction of the surface chemistry and pollutants of BS (Larkin 2011). Additionally, a high amount of these functional groups could influence the adsorption processes because of the hydrogen bonds formed between the water and oxygenated functional groups, which block the access of pollutants to the porosity of activated carbon (Alagarsamy 2011).

The physisorption isotherm was obtained for the optimal sample, R2-MNS. According to the BET model, it exhibited a surface area of $1225\text{ m}^2/\text{g}$, while the QS-DFT (Quenched State Density Functional Theory) surface area was slightly higher at $1239\text{ m}^2/\text{g}$. Additionally, R2-MNS displayed a pore volume of $0.801\text{ cm}^3/\text{g}$ and an average pore size of 0.463 nm . Figure 3a displays the isotherm shape of R2-MNS. Clearly, the isotherm shows a combination of Type II and IV accompanied by adsorption–desorption hysteresis of Type H4 according to IUPAC nomenclature. The characteristics of these isotherms are primarily composed of micropores and mesopores. The pore width presented in Fig. 3b shows two peaks, which correspond mainly to mesopores, with a small contribution of micropores, confirming the isotherm trend.

3.3 Effect of PH and determination of pH_{pzc}

It is well established that pH significantly influences the adsorption mechanism by regulating the charges on the adsorbent surface and participating in the degree of ionization of the solution components (Jeirani et al. 2017). On the other hand, the pH_{pzc} is the point when the surface charge on the activated carbon is neutral. In this work, the pH_{pzc} of R2-MNS is 4.5, indicating an acidic behaviour of this sample (Fig. 4a). At a pH higher than pH_{pzc} ($\text{pH} > 4.5$), the surface of R2-MNS is negatively charged and could promote affinity of the surface to attract more cations in the BS, i.e. the MB (Kılıç and Orhan 2019). When the pH is less than 4.5 the opposite phenomenon occurs and

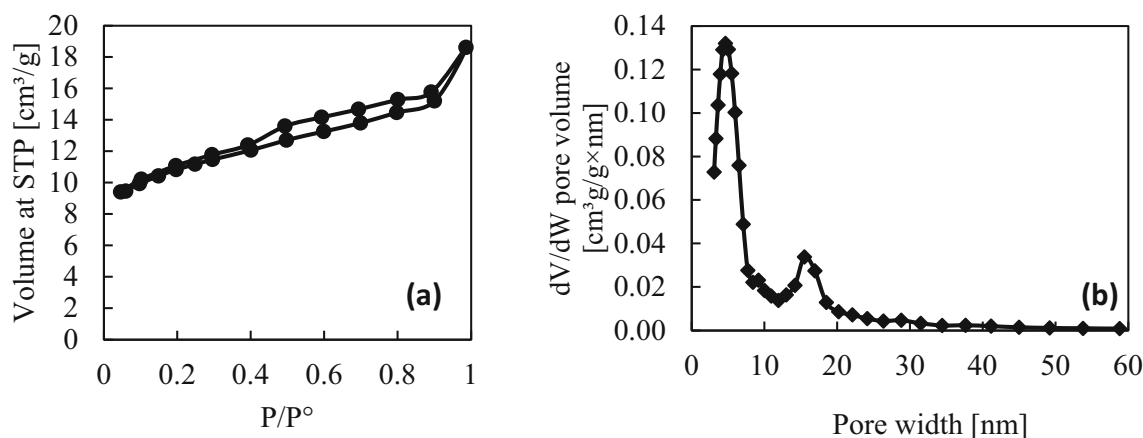


Fig. 3 **a** R2-MNS adsorption–desorption isotherm, and **b** pore size distribution following DFT methodology

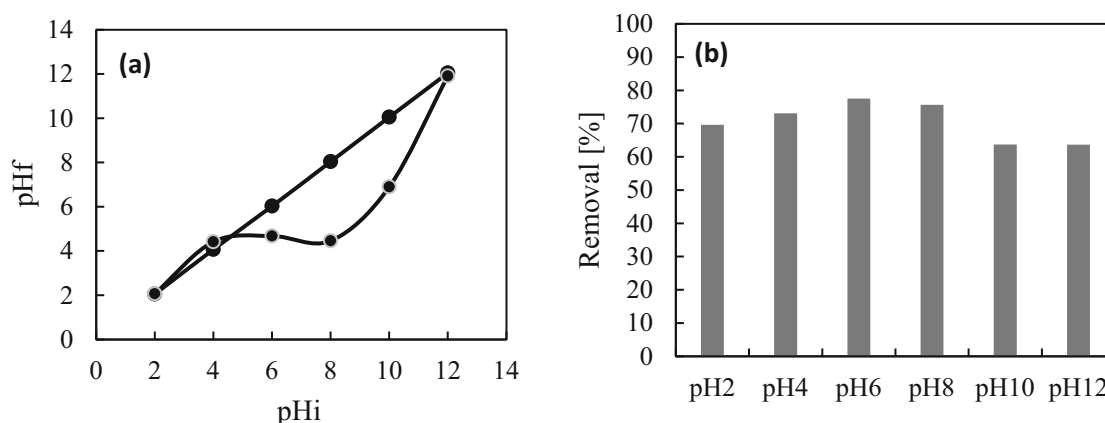


Fig. 4 Effect of pH in adsorption of BS. **a** Determination of pH_{pzc} for R2-MNS in BS, and **b** Percentage of binary solution removed at different pH values

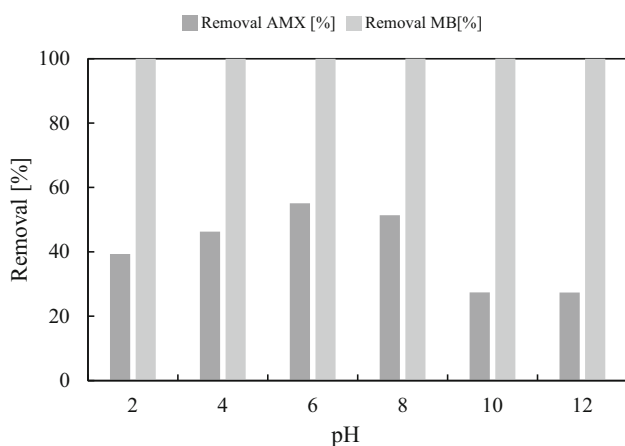


Fig. 5 Removal of each pollutant from BS at the corresponding pH

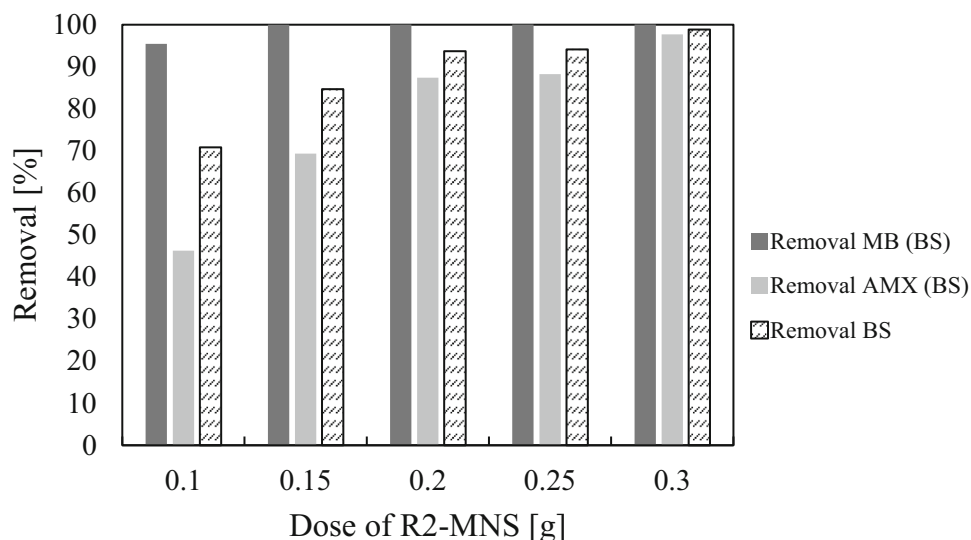
more anions would be preferably adsorbed on the carbon surface, in this case, represented by AMX.

Figure 4b illustrates the impact of the pH of the binary solution (BS) on the adsorption capacity, covering a pH

range from 2 to 12. The results distinctly indicate that R2-MNS exhibits favourable adsorption capacity across a broad pH spectrum; however, a notable decline in pollutant removal is observed in a highly alkaline environment. The optimum adsorption occurred at a pH of 6, achieving a 77.53% removal of BS (comprising 55.85% removal of AMX and 99.98% removal of MB). Conversely, the least effective behaviour was observed at pH 10 and 12, yielding 63.69% and 63.66% removal of BS, respectively.

Also, Fig. 5 shows the quantity of each component of BS adsorbed at different pH values. Evidently, there are no changes in MB removal percentage in all the tested pH range, which suggests that the forces involved here are mostly π - π interaction (Lyu et al. 2018; Esvandi et al. 2020). Also, this indicates that AMX has a synergistic behaviour towards MB, hence, it is not affected by the presence of AMX (Martínez et al. 2023). On the other hand, it is expected that AMX would have a better adsorption capacity at acidic pH, however, the optimal pH for AMX removal in BS was pH 6. Under acidic

Fig. 6 Effect of R2-MNS concentration on adsorption processes at 150 rpm for 12 h and room temperature



conditions, the AMX molecule is found in its negative form (with $-\text{COOH}$ already converted to $-\text{COO}^-$) and the surface of R2-MNS is positively charged ($\text{pH} < 4.5$), hence, the predominant adsorption mechanism is mainly through electrostatic forces (Homem et al. 2010). When the pH was increased, the surface of R2-MNS becomes negatively charged ($\text{pH} > 4.5$), which causes electrostatic repulsion of mentioned anions, and initiates a competitive adsorption process between the OH^- groups from the alkalinity of the solution and $-\text{COO}^-$ functional groups from AMX (Imanipoor et al. 2021).

3.4 Effect of R2-MNS dosage

The concentration of R2-MNS was varied from 0.10 to 0.30 g to investigate the effect of the adsorbent dose. The experiment was conducted using 100 mL of 400 mg/L of BS under 24 h as shown in Fig. 6. Notably, the percentage uptake was measured for each pollutant in parallel and simultaneously at their respective wavelengths. At a dosage of 0.10 g, a noticeable contrast in the uptake percentage between MB and AMX is evident. The removal percentages for MB and AMX are approximately 95% and 46%, respectively. Upon increasing the dosage of R2-MNS, the removal capacity for BS exhibits a linear increase. The adsorption of MB reaches 100% at the initial R2-MNS dose, and this saturation point is sustained even at higher doses. This phenomenon can be attributed to the higher affinity of MB for the activated carbon sample, resulting in its preferential adsorption, influenced by competitive adsorption dynamics. Consequently, AMX becomes available to be adsorbed at the remaining vacant active sites. In this context, the uptake of AMX by R2-MNS increases with an increase in the carbon dosage, indicating that additional active sites are still needed to effectively

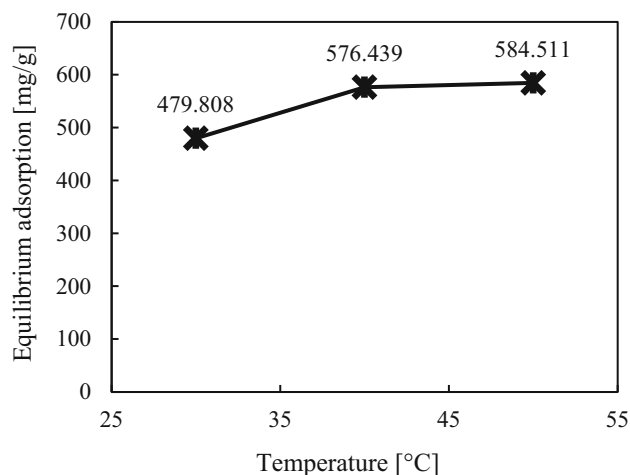


Fig. 7 Effect of temperature for BS adsorption with R2-MNS probed at 30, 40, and 50 °C, for 24 h and 150 rpm

remove AMX. In other words, the AMX adsorption is proportional to the concentration of R2-MNS. This process primarily occurs in the micropore region, where the greatest number of active sites for adsorption in aqueous solutions can be found. Considering the results and associated costs in producing activated carbon, a working dosage of 0.2 g was selected to carry out the rest of the experiments. This amount was chosen because the adsorbent shows an adequate adsorption capacity without spending lots of activated carbon.

3.5 Effect of temperature

Temperature is an important parameter that affects principally the rate and range of the adsorption. In this case, the influence of temperature was investigated from 30 to 50 °C and the result is shown in Fig. 7. Parameters such as pH,

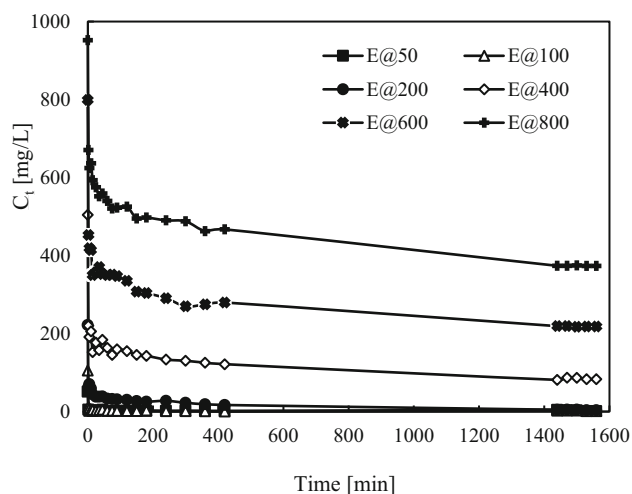


Fig. 8 Effect of contact time in the removal of BS using 0.2 g of R2-MNS at 40 °C, neutral pH

R2-MNS dosage, and concentration of BS were maintained at the optimal conditions already selected in previous sections (0.2 g of R2-MNS and neutral pH). Usually, an increase in temperature is expected to promote adsorption mechanisms (Bergmann et al. 2015). This is because increasing temperature decreases the viscosity and increases molecular motion allowing the pollutants to adsorb on the activated carbon. Above 40 °C, the equilibrium adsorption was slightly enhanced, approximately 10 mg/g. Further increase in temperature above 50 °C will promote the reversibility of the adsorption equilibrium (Foo and Hameed 2010). From the viewpoint of the input energy and resources employed, a temperature of 40 °C was selected as the best temperature for the rest of the experiments.

3.6 Effect of contact time and kinetic of adsorption

Sufficient contact time is crucial to ensure that the adsorbent reaches adsorption equilibrium. In this study, experiments were conducted at various concentrations of BS ranging from 50 to 800 mg/L. An equal proportion of AMX and MB in each experiment were consistently maintained. For instance, a 50 mg/L solution of BS was prepared by adding 25 mg/L of MB and 25 mg/L of AMX. Simultaneously, the optimal temperature (40 °C) and pH (neutral), as discussed in previous sections, were employed. Figure 8 shows that BS adsorption increases with time until equilibrium is reached. For all experiments, a notable trend was observed, characterized by robust adsorption initially, followed by a more gradual adsorption thereafter. Notably, at the lowest concentrations of BS (50 mg/L and 100 mg/L), equilibrium was achieved within the first 2 min. This rapid equilibrium can be attributed to the abundant free active sites present on the activated

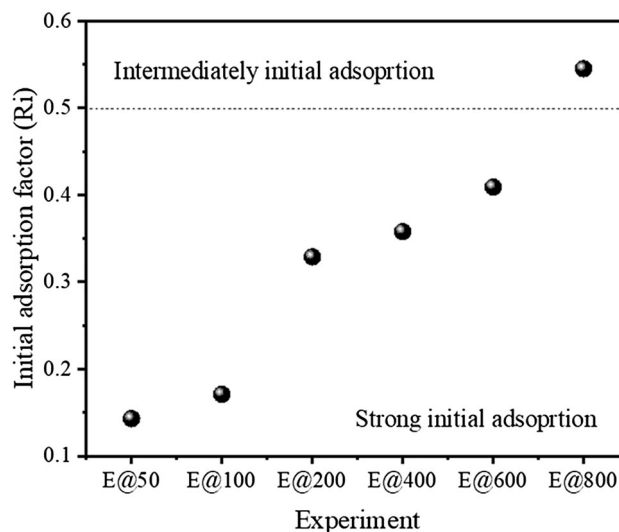


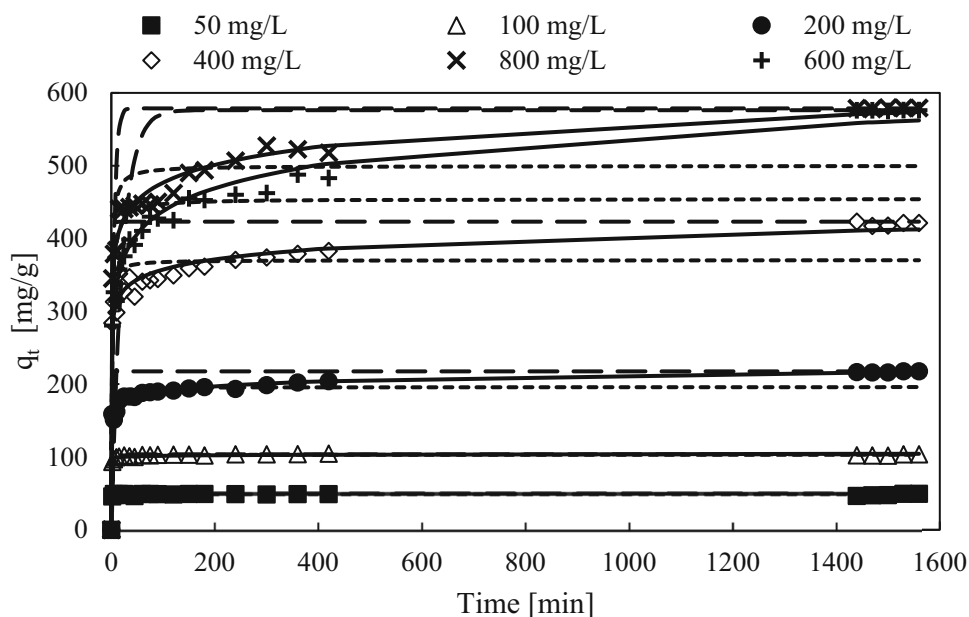
Fig. 9 Adsorption behaviour of adsorption experiments from Weber-Morris' methodology

carbon material. As the concentration increased from 200 to 800 mg/L, equilibrium was reached after 400 min. This prolonged equilibrium time corresponds to the saturation point of active sites on the adsorbent, considering the impact of competitive adsorption. The observed adsorption behaviour in these experiments can be interpreted as an initial intense adsorption phase, primarily driven by the availability of free active sites on the surface of R2-MNS.

Additionally, interparticle diffusion could support the adsorption rate of the samples. Using the initial adsorption factor (R_i) obtained from the Weber-Morris methodology (Weber and Morris 1962), it was found that experiments at concentrations from 50 to 600 mg/L of BS demonstrate strong initial adsorption (R_i value between 0.5 and 0.1), see Fig. 9. Meanwhile, at 800 mg/L the behaviour was described better as intermediately initial adsorption (R_i value between 0.9 and 0.5) (Wu et al. 2009).

On the other hand, it was also found that the maximum adsorption capacity at 40 °C was 578.925 mg/g from an initial concentration of 800 mg/L of BS in approximately 24 h. The experimental kinetic data were fitted with pseudo-first-order kinetic (PFO), pseudo-second-order kinetic (PSO), and Elovich models. The results of the fitting are shown in Fig. 10. Observably, the PSO model best described the variation in the experimental data followed by the Elovich and then PFO. This was validated by the range of coefficients of determination R^2 and the error analysis based on root-mean-square error (RMSE) and absolute relative error (ARE) at different initial BS concentrations (Table 3). The PFO has RMSE in the range of 1.511–109.502, ARE range of 0.022–0.225, and R^2 in the range of 0.991–0.842. The PSO presented RMSE, ARE, and R^2 ranges of 0.937–64.349, 0.015–0.103, and

Fig. 10 PFO, PSO, and Elovich kinetics modelling fitted to experimental data from different initial concentrations at 40 °C and neutral pH



0.999–0.869, respectively. Whereas, the Elovich model has RMSE of 1.032–14.472, ARE of 0.013–0.029, and R^2 of 0.997–0.991. The superior fit obtained from PSO compared to PFO implies that the interaction mechanism between R2-MNS and BS predominantly occurs through chemisorption. Additionally, the successful adaptation of the Elovich model to the kinetic data, characterized by minimal error and a high R^2 value, signifies heterogeneous adsorption on the surface of R2-MNS (Terdputtakun et al. 2017; Sahoo and Prelot 2020; Wang and Guo 2020; Revellame et al. 2020). It is worth noting that PSO performs well for low-concentration solutions, and this could be a primary reason for its less than perfect adaptation to the higher concentrations employed in this experimental study (Wang and Guo 2020).

3.7 Isotherm modelling

Adsorption isotherm models could be used to describe the interaction mechanism occurring between the R2-MNS and BS. Also, the parameters obtained from these models provide information on the values of maximum adsorption capacity, energy, surface properties, etc. (Bonilla-Petriciolet et al. 2017). In this study, eight isotherm models were evaluated, and the result was correlated and validated by R^2 .

The best fitting was Khan isotherm (followed by Freundlich, and Langmuir models) according to the R^2 value in all temperatures, which is close to unity (Table 4). Besides, the Khan isotherm model is a combined Langmuir and Temkin isotherm that has been specifically used for pure substances adsorption (bi-adsorbate adsorption), which is the phenomenon described in the present work

(Mozaffari Majd et al. 2022). In the same sense, the Freundlich isotherm reveals valuable insights into the characteristics of the adsorbent surface. In this instance, a value of $1/n_F < 1$ was obtained, as all the values for n_F (the strength constant) exceeded unity. This underscores the adsorbent's effectiveness when in contact with low-concentration solutions (Nguyen et al. 2022). Similarly, the Langmuir model is well-suited to elucidate the behaviour of the adsorption phenomena in these experiments. Conversely, the Langmuir isotherm characterizes homogeneous monolayer adsorption, assuming the absence of lateral interactions between the adsorbate and adsorbent (Kalam et al. 2021).

Additionally, separation factor (R_L) from this isotherm was evaluated at different temperatures and initial BS concentrations to study the nature of the adsorption process and to describe the affinity of BS molecules to the R2-MNS surface (Fig. 11). R_L values obtained were between 0 and 1, these values exponentially decrease as the initial concentration increases, indicating favourable adsorption (Al-Ghouti and Da'ana 2020). In addition, the adsorption intensity values ($1/n_F$) obtained in this work were less than zero in all temperatures, which indicates that the adsorption processes are favourable (Kalam et al. 2021).

3.8 Adsorption thermodynamics

The thermodynamics parameters in Table 5 could give an idea of the spontaneous or nonspontaneous nature of adsorption, and the viability of the adsorption process (Ray et al. 2020). The Gibb's free energy ($\Delta^\circ G$) enthalpy ($\Delta^\circ H$) and entropy ($\Delta^\circ S$) were obtained.

Table 3 Parameters and errors obtained from the adsorption kinetics models from real data

BS [mg/L]	q_e	Pseudo-first-order				Pseudo-second-order				Elovich							
		k_1	R^2	RMSE	ARE	$q_{e,cal}$	K_2	R^2	RMSE	ARE	$q_{e,cal}$	β	α	R^2	RMSE	ARE	
		$q_{e,cal}$															
50	49.452	49.452	0.946	0.991	1.511	0.022	48.544	0.212	0.996	0.937	0.015	48.619	10.235	8.292E + 211	0.995	1.032	0.018
100	103.665	103.665	0.512	0.965	5.801	0.024	103.093	0.043	0.999	1.000	0.008	104.449	0.978	1.5444E + 41	0.997	1.616	0.013
200	217.604	217.604	0.656	0.926	27.412	0.119	196.078	0.007	0.955	12.880	0.055	216.626	0.105	42.663,731.7	0.996	3.613	0.013
400	423.176	423.176	0.556	0.908	64.053	0.153	370.370	0.004	0.933	29.990	0.065	412.657	0.050	10.831,092.2	0.991	11.386	0.026
600	576.439	576.439	0.047	0.842	109.502	0.225	454.545	0.001	0.869	64.349	0.103	562.293	0.022	7104.40585	0.993	14.472	0.020
800	578.925	578.925	0.200	0.868	92.988	0.170	500.000	0.002	0.917	47.602	0.082	573.728	0.028	262,209.652	0.995	12.072	0.029

Table 4 Data obtained from evaluated isotherm models at different temperatures

	303 K	313 K	323 K
Langmuir			
q_m	416.666	666.667	555.556
K_L	0.3871	0.095	0.070
R_L	0.0519–0.0029	0.0484–0.0027	0.0519–0.0026
R^2	0.977	0.975	0.951
Freundlich			
n_F	4.488	2.835	2.788
K_F	136.899	84.217	73.164
R^2	0.982	0.970	0.951
Khan			
q_m	137.659	261.775	243.074
K_K	10.774	0.439	0.355
n_K	0.851	0.839	0.832
R^2	0.992	0.988	0.964

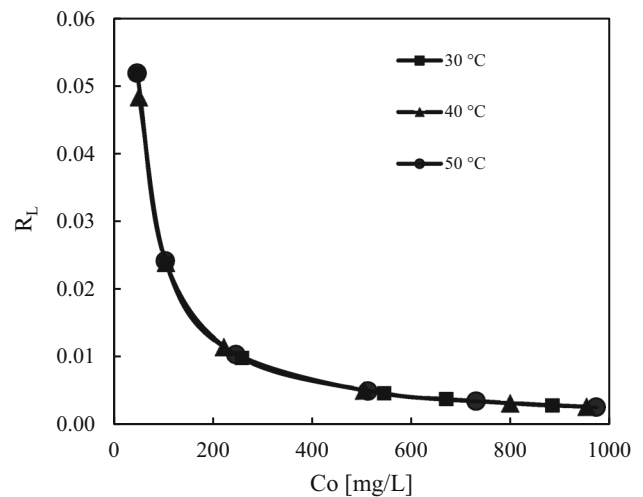


Fig. 11 Separation factor evaluated at different temperatures

Table 5 Thermodynamics parameters of the adsorption process

T [K]	ΔG [kJ/mol]	ΔS [J/mol]	ΔH [kJ/mol]
303	1.038		
313	2.661	– 104.38	– 30.404
323	3.101		

The negative value of enthalpy (– 30.404 kJ/mol) suggests exothermic adsorption, whereas the negative value of entropy (– 104.38 J/mol) indicates less disorder in the process. For Gibb’s energy ($\Delta^\circ G$), positives values of 1.038 kJ/mol, 2.661 kJ/mol, and 3.101 kJ/mol, were

Table 6 Adsorption capacity comparisons with adsorbents made from macadamia nutshell

References	Pollutant	Activation method	Removal capacity (mg/g)
Wongcharee and Aravinthan (2020)	Melanoidin	–	14.7
Wongcharee et al. (2019)	Methylene Blue	Physical activation	97
Wongcharee et al. (2018)	Methylene Blue	Physical activation	134.69
Du et al. (2017)	Reactive Blue 19	Chemical activation (KOH)	376.81
Jiang et al. (2017)	Methylene Blue	–	444.732
Wongcharee et al. (2017)	Methylene Blue	Physical activation	41.83
Martins et al. (2015)	Tetracycline	Chemical activation (NaOH)	455.33
This work	Methylene Blue and Amoxicillin	Chemical activation (K ₂ CO ₃)	578.925

obtained at temperatures of 303 K, 313 K and 323 K, respectively, indicating a nonspontaneous reaction (Ebelegi et al. 2020). Additionally, the activation energy value calculated through the Arrhenius equation was 51.68 kJ/mol, which means that the process involved in this work was essentially chemisorption (Inglezakis and Zorpas 2012).

Table 6 provides knowledge about previous recent works where macadamia nutshell was used as a precursor. Data presented in the table contains information regarding the maximum removal capacity reached through using their methods for primarily one pollutant, which in all cases are lesser than the results shown in the presented work.

4 Conclusions

In conclusion, microporous activated carbon was developed from macadamia nutshell using potassium carbonate as an eco-friendly activation agent. The Box–Behnken toolbox allowed for the generation of experimental design (15 experimental runs) to evaluate the influence of factors such as K₂CO₃:precursor ratio, activation temperature, and activation time on the response surface for binary adsorption of cationic methylene blue dye and ionic amoxicillin antibiotics. Under optimal conditions of 900 °C, 1 h, and K₂CO₃:precursor ratio of 2:1, the R2-MNS revealed a specific surface area of 1225 m²/g, pore volume of 0.801 cm³/g, and an average pore width of 0.406 nm. The R2-MNS activated carbon realized a maximum adsorption capacity of 578.9 mg/g under the best conditions of 40 °C and neutral pH. The pseudo-second-order adsorption kinetic model adequately described the experimental data with RMSE, ARE, and R² in the range of 0.937–64.349, 0.015–0.103, and 0.999–0.869, which indicates a chemisorption mechanism. Evaluated isotherm models revealed that Khan isotherm used for pure substances best described the variation in the data. Thermodynamic studies

show exothermic adsorption. Overall, value-added activated carbon can be derived from macadamia nutshell for multipollutant removal in a single stage adsorption. Studies on waste integration for activated carbon production and atomistic evaluation of possible interactions of the pollutants in the solution is recommended to enhance the understanding of this process.

Acknowledgements The authors of this work gratefully acknowledge the technical support of R. Morán-Elvira for help with SEM and EDS analysis and R. Nava-Lara for FTIR analysis. This work was financially supported by Dirección General de Asuntos del Personal Académico, Mexico under Programa de Apoyo a Proyectos de Investigación e Innovación Tecnológica (DGAPA-PAPIIT) Project Nos: IA102522. Estefania Duque-Brito received a fellowship from CONAHCYT.

Declarations

Conflict of interest The authors declare that they have no known competing financial interests or personal relationships that could have appeared to influence the work reported in this paper.

Open Access This article is licensed under a Creative Commons Attribution 4.0 International License, which permits use, sharing, adaptation, distribution and reproduction in any medium or format, as long as you give appropriate credit to the original author(s) and the source, provide a link to the Creative Commons licence, and indicate if changes were made. The images or other third party material in this article are included in the article's Creative Commons licence, unless indicated otherwise in a credit line to the material. If material is not included in the article's Creative Commons licence and your intended use is not permitted by statutory regulation or exceeds the permitted use, you will need to obtain permission directly from the copyright holder. To view a copy of this licence, visit <http://creativecommons.org/licenses/by/4.0/>.

References

- Aichour A, Zaghoulane-Boudiaf H (2020) Single and competitive adsorption studies of two cationic dyes from aqueous mediums onto cellulose-based modified citrus peels/calcium alginate composite. *Int J Biol Macromol* 154:1227–1236. <https://doi.org/10.1016/j.ijbiomac.2019.10.277>

- Alagarsamy G (2011) Industrial sludge based adsorbents/industrial by-products in the removal of reactive dyes—a review. *Int J Water Resour Environ Eng* 3:1–9
- Al-Ghouti MA, Da'ana DA (2020) Guidelines for the use and interpretation of adsorption isotherm models: a review. *J Hazard Mater* 393:122383. <https://doi.org/10.1016/J.JHAZMAT.2020.122383>
- Al-Ghouti MA, Sweleh AO (2019) Optimizing textile dye removal by activated carbon prepared from olive stones. *Environ Technol Innov* 16:100488. <https://doi.org/10.1016/J.ETI.2019.100488>
- Bergmann CP, Machado F, Editors M (2015) Carbon nanostructures carbon nanomaterials as adsorbents for environmental and biological applications, 1st edn. Springer International Publishing Switzerland. <https://doi.org/10.1007/978-3-319-18875-1>
- Bonilla-Petriciolet A, Mendoza-Castillo DI, Reynel-Ávila HE (2017) Adsorption processes for water treatment and purification. Springer International Publishing. <https://doi.org/10.1007/978-3-319-58136-1>
- Borghesi SA, Zare MH, Ahmadi M, et al (2021) Synthesis of multi-application activated carbon from oak seeds by KOH activation for methylene blue adsorption and electrochemical supercapacitor electrode. *Arabian J Chem*. <https://doi.org/10.1016/j.arabjc.2020.102958>
- Bouzidi M, Sellaoui L, Mohamed M et al (2023) A comprehensive study on paracetamol and ibuprofen adsorption onto biomass-derived activated carbon through experimental and theoretical assessments. *J Mol Liq* 376:121457. <https://doi.org/10.1016/J.MOLLIQ.2023.121457>
- Chandrasekaran A, Patra C, Narayanasamy S, Subbiah S (2020) Adsorptive removal of ciprofloxacin and amoxicillin from single and binary aqueous systems using acid-activated carbon from *Prosopis juliflora*. *Environ Res* 188:109825. <https://doi.org/10.1016/J.ENVRRES.2020.109825>
- da Silva Santos DH, Paulino JCPL, dos Santos Alves GF et al (2021) Effluent treatment using activated carbon adsorbents: a bibliometric analysis of recent literature. *Environ Sci Pollut Res* 28:32224–32235
- Dao TM, Le Luu T (2020) Synthesis of activated carbon from macadamia nutshells activated by H_2SO_4 and K_2CO_3 for methylene blue removal in water. *Bioresour Technol Rep* 12:100583. <https://doi.org/10.1016/J.BITEB.2020.100583>
- Du C, Xue Y, Wu Z, Wu Z (2017) Microwave-assisted one-step preparation of macadamia nut shell-based activated carbon for efficient adsorption of reactive blue. *New J Chem* 41:15373–15383. <https://doi.org/10.1039/c7nj03208k>
- Ebelegi AN, Ayawei N, Wankasi D (2020) Interpretation of adsorption thermodynamics and kinetics. *Open J Phys Chem* 10:166–182. <https://doi.org/10.4236/ojpc.2020.103010>
- Elovich SY, Larinov OG (1962) Theory of adsorption from solutions of non electrolytes on solid (I) equation adsorption from solutions and the analysis of its simplest form, (II) verification of the equation of adsorption isotherm from solutions. *Izvestiya Akademii Nauk* 2:209–216
- Esvandi Z, Foroutan R, Peighambardoust SJ et al (2020) Uptake of anionic and cationic dyes from water using natural clay and clay/starch/MnFe₂O₄ magnetic nanocomposite. *Surf Interf*. <https://doi.org/10.1016/j.surfin.2020.100754>
- Figueiredo JL, Pereira MFR (2012) Porous texture versus surface chemistry in applications of adsorption by carbons in Novel Carbon Adsorbent. pp. 471–498. <https://doi.org/10.1016/B978-0-08-097744-7.00015-6>
- Foo KY, Hameed BH (2010) Insights into the modeling of adsorption isotherm systems. *Chem Eng J* 156:2–10. <https://doi.org/10.1016/j.cej.2009.09.013>
- Freundlich HMF (1906) Over the adsorption in solution. *J Phys Chem* 57:385
- Gupta SA, Vishesh Y, Sarvshrestha N et al (2022) Adsorption isotherm studies of Methylene blue using activated carbon of waste fruit peel as an adsorbent. *Mater Today Proc* 57:1500–1508. <https://doi.org/10.1016/j.matpr.2021.12.044>
- Ho YS, Mckay G (1999) Pseudo-second order model for sorption processes
- Homem V, Alves A, Santos L (2010) Amoxicillin removal from aqueous matrices by sorption with almond shell ashes1. *Int J Environ Anal Chem* 90:1063–1084. <https://doi.org/10.1080/03067310903410964>
- Iftekhhar S, Heidari G, Amanat N et al (2022) Porous materials for the recovery of rare earth elements, platinum group metals, and other valuable metals: a review. *Environ Chem Lett* 20:3697–3746
- Imanipoor J, Mohammadi M, Dinari M, Ehsani MR (2021) Adsorption and desorption of amoxicillin antibiotic from water matrices using an effective and recyclable MIL-53(Al) metal-organic framework adsorbent. *J Chem Eng Data* 66:389–403. <https://doi.org/10.1021/acs.jced.0c00736>
- Inglezakis VJ, Zorpas AA (2012) Heat of adsorption, adsorption energy and activation energy in adsorption and ion exchange systems. *Desalination Water Treat* 39:149–157. <https://doi.org/10.1080/19443994.2012.669169>
- Ismail WNW, Syah MIAI, Muhet NHA, et al (2022) Adsorption behavior of heavy metal ions by hybrid inulin-TEOS for water treatment. *Civil Eng J*. 8:1787–1798. <https://doi.org/10.28991/CEJ-2022-08-09-03>
- Jeirani Z, Niu CH, Soltan J (2017) Adsorption of emerging pollutants on activated carbon. *Rev Chem Eng* 33:491–522. <https://doi.org/10.1515/revce-2016-0027>
- Jiang Y, Ye J, Feng Q, Yang W (2017) Exploration and optimization for methylene blue dye removal with modified macadamia nut shell. *Desalination Water Treat* 95:295–307. <https://doi.org/10.5004/dwt.2017.0276>
- Kalam S, Abu-Khamsin SA, Kamal MS, Patil S (2021) Surfactant adsorption and adsorption isotherms. *Adsorption* 6:32342–32348. <https://doi.org/10.1021/acsoomega.1c04661>
- Kılıç A, Orhan R (2019) Removal of cationic dyes by adsorption in a single and binary system using activated carbon prepared from the binary mixture. *Separat Sci Technol* 54:2147–2163. <https://doi.org/10.1080/01496395.2019.1636068>
- Lagergren S (1907) About the theory of so-called adsorption of soluble substances (Zur theorie der sogenannten adsorption gelöster Stoffe). *Zeitschrift für Chemie und Industrie der Kolloide* 2
- Lang J, Matějová L, Cuentas-Gallegos AK et al (2021) Evaluation and selection of biochars and hydrochars derived from agricultural wastes for the use as adsorbent and energy storage materials. *J Environ Chem Eng* 9:105979. <https://doi.org/10.1016/J.JECE.2021.105979>
- Langmuir I (1916) The constitution and fundamental properties of solids and liquids. Part I. Solids. *J Am Chem Soc* 38:2221–2295. <https://doi.org/10.1021/ja02268a002>
- Larkin P (2011) Infrared and Raman spectroscopy. Principles and spectral interpretation, 1st edn. Elsevier
- Lazarotto JS, Schnorr C, Georgin J et al (2022) Microporous activated carbon from the fruits of the invasive species *Hovenia dulcis* to remove the herbicide atrazine from waters. *J Mol Liq*. <https://doi.org/10.1016/j.molliq.2022.120014>
- Leite AB, Saucier C, Lima EC et al (2018) Activated carbons from avocado seed: optimisation and application for removal of several emerging organic compounds. *Environ Sci Pollut Res* 25:7647–7661. <https://doi.org/10.1007/s11356-017-1105-9>
- Liu P, Song T, Deng R et al (2023) The efficient removal of congo red and ciprofloxacin by peony seeds shell activated carbon with ultra-high specific surface area. *Environ Sci Pollut Res* 30:53177–53190. <https://doi.org/10.1007/s11356-023-26146-7>

- Lyu H, Gao B, He F et al (2018) Experimental and modeling investigations of ball-milled biochar for the removal of aqueous methylene blue. *Chem Eng J* 335:110–119. <https://doi.org/10.1016/J.CEJ.2017.10.130>
- Malesic-Eleftheriadou N, Liakos EV, Evgenidou E et al (2022) Low-cost agricultural wastes (orange peels) for the synthesis and characterization of activated carbon biosorbents in the removal of pharmaceuticals in multi-component mixtures from aqueous matrices. *J Mol Liq* 368:120795. <https://doi.org/10.1016/J.MOLLIQ.2022.120795>
- Martínez RJ, Vela-Carrillo AZ, Godínez LA et al (2023) Competitive adsorption of anionic and cationic molecules on three activated carbons derived from agroindustrial waste. *Biomass Bioenergy* 168:106660. <https://doi.org/10.1016/J.BIOMBIOE.2022.106660>
- Martins AC, Pezoti O, Cazetta AL et al (2015) Removal of tetracycline by NaOH-activated carbon produced from macadamia nut shells: kinetic and equilibrium studies. *Chem Eng J* 260:291–299. <https://doi.org/10.1016/J.CEJ.2014.09.017>
- Moura FCC, Rios RDF, Galvão BRL (2018) Emerging contaminants removal by granular activated carbon obtained from residual Macauba biomass. *Environ Sci Pollut Res* 25:26482–26492. <https://doi.org/10.1007/s11356-018-2713-8>
- Mozaffari Majd M, Kordzadeh-Kermani V, Ghalandari V, et al (2022) Adsorption isotherm models: a comprehensive and systematic review (2010–2020). *Sci Total Environ* 812:151334. <https://doi.org/10.1016/j.scitotenv.2021.151334>
- Nematov DD, Kholmurodov KT, Husenzoda MA, et al (2022) Molecular Adsorption of H₂O on TiO₂ and TiO₂:Y Surfaces. *J Human Earth Fut* 3:213–222. <https://doi.org/10.28991/HEF-2022-03-02-07>
- Nguyen TD, Nguyen TMP, Van HT et al (2022) Adsorption removal of ammonium from aqueous solution using Mg/Al layered double hydroxides-zeolite composite. *Environ Technol Innov*. 25:102244. <https://doi.org/10.1016/j.eti.2021.102244>
- Nworie FS, Mgbemena N, Ike-Amadi AC, Eburnoha J (2022) Functionalized biochars for enhanced removal of heavy metals from aqueous solutions: mechanism and future industrial prospects. *J Human Earth Fut*. 3:377–395. <https://doi.org/10.28991/HEF-2022-03-03-09>
- Paul Nayagam JO, Prasanna K (2022) Utilization of shell-based agricultural waste adsorbents for removing dyes: a review. *Chemosphere* 291, 132737. <https://doi.org/10.1016/j.chemosphere.2021.132737>
- Pezoti O, Cazetta AL, Bedin KC et al (2016) NaOH-activated carbon of high surface area produced from guava seeds as a high-efficiency adsorbent for amoxicillin removal: kinetic, isotherm and thermodynamic studies. *Chem Eng J* 288:778–788. <https://doi.org/10.1016/J.CEJ.2015.12.042>
- Putra EK, Pranowo R, Sunarso J et al (2009) Performance of activated carbon and bentonite for adsorption of amoxicillin from wastewater: mechanisms, isotherms and kinetics. *Water Res* 43:2419–2430. <https://doi.org/10.1016/J.WATRES.2009.02.039>
- Qin Q, Wu X, Chen L et al (2018) Simultaneous removal of tetracycline and Cu(II) by adsorption and coadsorption using oxidized activated carbon. *RSC Adv* 8:1744–1752. <https://doi.org/10.1039/c7ra12402c>
- Ray SS, Gusain R, Kumar N (2020) Adsorption equilibrium isotherms, kinetics and thermodynamics. In: *Carbon nanomaterial-based adsorbents for water purification*. Elsevier, pp 101–118
- Revellame ED, Fortela DL, Sharp W et al (2020) Adsorption kinetic modeling using pseudo-first order and pseudo-second order rate laws: a review. *Clean Eng Technol* 1:100032. <https://doi.org/10.1016/J.CLET.2020.100032>
- Rodrigues DLC, Machado FM, Osório AG et al (2020) Adsorption of amoxicillin onto high surface area-activated carbons based on olive biomass: kinetic and equilibrium studies. *Environ Sci Pollut Res* 27:41394–41404. <https://doi.org/10.1007/s11356-020-09583-6>
- Sahoo TR, Prelot B (2020) Adsorption processes for the removal of contaminants from wastewater: The perspective role of nanomaterials and nanotechnology. In: *Nanomaterials for the detection and removal of wastewater pollutants*. Elsevier, pp 161–222
- SAMAC. Macadamias South Africa NPC (2023) Industry Statistics. <https://samac.org.za/industry-statistics/#:~:text=Macadamia%20Production,8%2019%20tonnes%20in%202023>. Accessed 5 Sep 2023
- Servicio de Información Agroalimentaria y Pesquera (2023) Estadísticas de producción agrícola. <http://infosiap.siap.gob.mx/gobmx/datosAbiertos.php>. Accessed 5 Sep 2023
- Suárez C, Gudíol F (2009) Beta-lactam antibiotics. *Enferm Infecc Microbiol Clin* 27:116–129. <https://doi.org/10.1016/j.eimc.2008.12.001>
- Sun Y, Darling AJ, Li Y et al (2019) Defect-mediated selective hydrogenation of nitroarenes on nanostructured WS₂. *Chem Sci* 10:10310–10317. <https://doi.org/10.1039/c9sc03337h>
- Terdputtakun A, Arqueropanyo O, Sooksamit P et al (2017) Adsorption isotherm models and error analysis for single and binary adsorption of Cd(II) and Zn(II) using leonardite as adsorbent. *Environ Earth Sci*. <https://doi.org/10.1007/s12665-017-7110-y>
- Wang J, Guo X (2020) Adsorption kinetic models: physical meanings, applications, and solving methods. *J Hazard Mater*. 390:122156. <https://doi.org/10.1016/j.jhazmat.2020.122156>
- Weber WJ, Morris JC (1962) Advances in water pollution research: removal of biologically resistant pollutant from waste water by adsorption. In: *Proceedings of 1st international conference on water pollution symposium*. Pergamon Press 2:231–266
- Wei M, Marrakchi F, Yuan C et al (2022) Adsorption modeling, thermodynamics, and DFT simulation of tetracycline onto mesoporous and high-surface-area NaOH-activated macroalgae carbon. *J Hazard Mater*. 425:127887. <https://doi.org/10.1016/j.jhazmat.2021.127887>
- Wong S, Yac'cob NAN, Ngadi N et al (2018) From pollutant to solution of wastewater pollution: synthesis of activated carbon from textile sludge for dye adsorption. *Chin J Chem Eng* 26:870–878. <https://doi.org/10.1016/J.CJCHE.2017.07.015>
- Wongcharee S, Aravinthan V (2020) Application of mesoporous magnetic nanosorbent developed from macadamia nut shell residues for the removal of recalcitrant melanoidin and its fractions. *Separat Sci Technol* 55:1636–1649. <https://doi.org/10.1080/01496395.2019.1606015>
- Wongcharee S, Aravinthan V, Erdei L, Sanongraj W (2017) Use of macadamia nut shell residues as magnetic nanosorbents. *Int Biodeterior Biodegradation* 124:276–287. <https://doi.org/10.1016/J.IBIOD.2017.04.004>
- Wongcharee S, Aravinthan V, Erdei L, Sanongraj W (2018) Mesoporous activated carbon prepared from macadamia nut shell waste by carbon dioxide activation: comparative characterisation and study of methylene blue removal from aqueous solution. *Asia-Pacific J Chem Eng*. <https://doi.org/10.1002/apj.2179>
- Wongcharee S, Aravinthan V, Erdei L (2019) Mesoporous activated carbon-zeolite composite prepared from waste macadamia nut shell and synthetic faujasite. *Chin J Chem Eng* 27:226–236. <https://doi.org/10.1016/J.CJCHE.2018.06.024>
- World Health Organization (2018) Report on surveillance of antibiotic consumption
- Wu FC, Tseng RL, Juang RS (2009) Initial behavior of intraparticle diffusion model used in the description of adsorption kinetics. *Chem Eng J* 153:1–8. <https://doi.org/10.1016/J.CEJ.2009.04.042>
- Xue H, Wang X, Xu Q et al (2022) Adsorption of methylene blue from aqueous solution on activated carbons and composite prepared from an agricultural waste biomass: a comparative study by experimental and advanced modeling analysis. *Chem Eng J* 430:132801. <https://doi.org/10.1016/J.CEJ.2021.132801>

Yazidi A, Atrous M, Edi Soetaredjo F et al (2020) Adsorption of amoxicillin and tetracycline on activated carbon prepared from durian shell in single and binary systems: experimental study and modeling analysis. *Chem Eng J.* 379:122320. <https://doi.org/10.1016/j.cej.2019.122320>

Zhu Y, Kolar P, Shah SB et al (2018) Simultaneous mitigation of p-cresol and ammonium using activated carbon from avocado seed. *Environ Technol Innov* 9:63–73. <https://doi.org/10.1016/J.ETI.2017.10.006>